

CAAP Quarterly Report

Date of Report: July 10th 2020

Prepared for: *U.S. DOT Pipeline and Hazardous Materials Safety Administration*

Contract Number: 693JK31850008CAAP

Project Title: Fluorescent Chemical Sensor Array for Detecting and Locating Pipeline Internal Corrosive Environment

Prepared by: Dr. Ying Huang, Dr. Wenfang Sun, and Dr. Hao Wang

Contact Information: Dr. Ying Huang, Email: ying.huang@ndsu.edu, Phone: 701.231.7651

For quarterly period ending: July 10th 2020

Business and Activity Section

(a) Contract Activity

Discussion about contract modifications or proposed modifications:

Proposed modification: The requested “No Cost Extension” to December 31 2021_instead of completing the project in September 31 2021 was approved. As explained in last quarterly report, this report was greatly impacted by the COVID-19 and no lab tests were performed in chemistry department, so this quarterly report was focused on literature review on Task 3. NDSU planned to re-open for the fall semester, if everything goes well after the re-open, the project is expected to resume to normal in next quarter.

Discussion about materials purchased:

None.

(b) Status Update of Past Quarter Activities

Task 3

(c) Cost share activity

Tuition Waiver for two graduate students with \$2,400 of cost share in this quarter.

(d) Task 3: Corrosion Model for Corrosion Prediction

In this quarter, we focused on literature review of the Task 3 (Corrosion Model for Corrosion Prediction) including the review of co-work mechanism of CO₂ and H₂S gas with pH value, and review of empirical CR model of H₂S gas. The detail findings are described as below.

1. Background and Objectives in the 7th Quarter

1.1 Background

This project is designed to develop passive colorimetric/fluorescent chemical sensor array for locating and detecting corrosive water inside pipes. Inside the pipelines, the transported crude oil may include a hot mixture of free water, carbon dioxide (CO₂), hydrogen sulfide (H₂S) and microorganisms. The different chemical components inside oil/water environment such as HCO₃⁻ / CO₃²⁻, Fe³⁺, S²⁻, H⁺ or pH may result in different internal corrosion mechanisms, such as sweet corrosion or sour corrosion. The passive colorimetric sensor array to be developed in this project is intended to detect the concentration changes of the five above mentioned important chemical species in the internal oil/water environment of the pipeline and use these detected environmental data to predict the internal corrosion progressing of pipelines.

1.2 Objectives in the 7th Quarter

In this quarter, to search for a reference of the empirical Corrosion Rate (CR) model, literature review work has been done to summarize previous research on applicable models on our target agent S²⁻. Accordingly, further application of prototype models and necessary experimental tests on specific parameter determination can be done. In addition, to integrate the majorities of possible corrosive agents, a better understanding of the co-work mechanism between S²⁻, CO₃²⁻/HCO₂⁻, and pH(H⁺) is also considered. Based on the literature review, a summarized global CR prediction model can be formulized for future laboratory experiments.

2. Results and Discussions

2.1 Integration of Corrosive Water into Internal Corrosion Prediction Models (Task 3)

Due to impact of COVID-19, we could not perform the tasks planned in last quarter. Thus, in this quarter, we performed a systematic literature review of Task 3.

2.1.1 Literature review on Corrosion Model under existence of CO₂ and H₂S

Corrosion in gas/liquid pipelines has been reported in the presence of H₂S and CO₂ in the gas and high chloride concentrations or sulfur/polysulfide sludge from the formation water and is believed to take place under the existence of O₂. Unfortunately, a O₂ free transporting demands a great deal of technical effort and seems impossible in modern pipeline industry. While single O₂ induced corrosion of gas transmission or pipelines has not been reported, a wide range of O₂ concentration limits can be found in the gas industry. A survey of 44 natural gas transmission pipeline companies indicated that the gas quality specifications allowed maximum O₂ concentrations ranging from < 10 vol% to 1.0 vol% [1]. Based on the American standard, the maximum allowance of O₂ content in gas pipelines is 0.2% by volume. The actual concentrations of O₂ in the gas stream were even lower as 0 vol% to 0.02 vol%. However, the typical O₂ concentrations in the natural gas pipelines are believed to be rising, particularly in lines transporting gases pumped from storage fields and from fields being produced under vacuum. The effects of water chemistry and gas composition on corrosion through thermodynamic and kinetic analyses have been examined through a combination of experimental investigation and thermodynamic modeling.

Dissolved CO₂ is converted into carbonic acid (H₂CO₃) inside pipelines especially the ones transporting liquid product, which then increases the cathodic reaction kinetics by dissociation to bicarbonate. Under stagnant conditions, dissolved ferrous ions combine with the H₂CO₃ to form ferrous carbonate (siderite; FeCO₃). However, under flow conditions, parts of the FeCO₃ scale may be removed, resulting in an increased corrosion rate of the steel attributable to the H₂CO₃. DeWaard and Milliams developed a semi-empirical correlation between corrosion rate under flowing conditions (\approx 1 m/s at the metal surface) and CO₂ partial pressure [2, 3], which the relation between the CR and the CO₂ partial pressure can be

presented as:

$$\log(CR/mm \cdot year^{-1}) = 5.8 - \frac{1780}{T} + 0.67 \log(pCO_2) \quad (\text{Eq.1})$$

Equation 1 provides a conservative estimate of corrosion rate under flowing conditions because it does not take account for the effect of nonideality of the gas phase and scale formation. The effect of total pressure of gas and FeCO₃ scale formation on decreasing the corrosion rate was given in terms of correction factors [3]. One of the major limitations of this approach is that the correction factors attributable to scale formation, pH, and total iron concentration are not considered in terms of a consistent thermodynamic speciation model. Other correlations have been presented in a recent review of the literature that apply to flow solutions containing a CO₂/H₂S ratio > 200 although no fundamental is provided for this cut-off in the ratio. Pitting corrosion was observed when the pH was allowed to attain its natural value 4 whereas no pitting corrosion was seen when the pH was controlled at a value of 6 using bicarbonate [4].

For the corrosion induced by sulfur (S), majority of the researches have revealed that H₂S in the gas stream is generally believed to be beneficial because of the formation of a protective iron sulfide film. Shoesmith, et al., examined the behavior of iron and steel in aqueous sulfide solutions because of its importance to the Girdler-Sulfide process used to produce heavy water in the Canadian nuclear program [5, 6]. In strongly alkaline conditions, steel was passivated by an oxide film that might have contained deposited sulfur in the pores, but no sulfide was detected. In solutions of pH ranging from 9 to 12, mackinawite (Fe_{1+x}S) formed after initial oxidation of steel. The total sulfide concentration in these investigations ranged from 0.04 M to 0.5 M. The mackinawite film was not completely protective and tended to flake off as it thickened [6]. Iron sulfides are known to increase the corrosion rate of steel. The iron sulfides and their crystal structures are given in Table 1.

Table 1 Types of Iron Sulfides and their Crystal Structures

Sulfide type	Chemical Formula	Stoichiometry	Crystal Structure
Mackinawite	Fe _{1+x} S	x = 0.057-0.064	Tetragonal
Pyrrhotite	Fe _{1-x} S	x = 0 to 0.14	Variable
Greigite	Fe ₃ S ₄	/	Cubic
Smythite	Fe _{3+x} S ₄	x = 0 to 0.25	Hexagonal
Pyrite	FeS ₂	S or Fe deficient	Cubic
Marcasite	FeS ₂	S deficient, unstable	Orthorhombic

Smith and Miller reviewed the effects of various iron sulfide compounds on the corrosion of iron in aqueous solutions [7]. Their work concluded the following findings:

- (a) Although iron sulfide was thermodynamically predicted to form over a wider range of pH and potential than iron oxide, iron sulfide film was generally not as protective as iron oxide and a more negative cathodic protection potential was required to protect steel in the presence of mackinawite than was generally considered adequate for steel.
- (b) The protectiveness of sulfide scale depended on the sulfide concentration in the aqueous solution and pH. For example, protective pyrrhotite (Fe_{1-x}S) scale was reported in the range of 15 ppm to 1,700 ppm whereas nonprotective mackinawite was observed above this concentration and in the pH range of 6.5 to 8.8.
- (c) The corrosiveness of iron sulfide depended on the aqueous solution chemistry. In distilled water

saturated with H₂S, a nonprotective mackinawite scale was formed initially but transformed to a protective pyrrhotite and pyrite (FeS₂) scale. In the presence of brine and CO₂, only a nonprotective mackinawite scale was formed. The corrosion rate continued to increase in the presence of brine.

- (d) In an aqueous solution with iron sulfide suspensions and on an equal molar basis, pyrite was found to be the most corrosive, followed by smythite, greigite (Fe₃S₄), mackinawite, and pyrrhotite. The corrosivity was found to be proportional to the sulfur to iron ratio of these compounds (Table 1). It was also found that sulfides produced a strong depolarization of the metal surface, which counteracted the protectiveness of the film. Thus, any defect in the film is likely to enhance the corrosion rate of the steel considerably.

Shoesmith, et al., using galvanostatic tests in aqueous solutions saturated with H₂S, showed that between pH of 4 and 7 the corrosion product consists of mostly mackinawite, and this layer is protective at first but becomes more porous with time [8]. It was observed that, in these solutions, the potential initially increases corresponding to film formation, then decreases corresponding to disruption, and then stays constant. Huang, et al., observed that saturation of a 4 wt% sodium chloride (NaCl) solution by H₂S resulted in an overall decrease in corrosion rate of steel, attributable to sulfide precipitation, but increased the corrosion of the ferrite phase because of preferential cathodic reactions on the iron sulfide [9]. A recent investigation has shown that, in the absence of iron sulfide formation, small additions of H₂S (up to 30 mmol) accelerate the dissolution rate of steel [10]. Thus, from the literature, it appears that iron sulfide scales protect corrosion of steel only under a limited set of conditions and that any defect in the film is likely to exacerbate the corrosion considerably.

Considering that there are two corrosion sources, a combination of CO₂ and H₂S effects was also studied. The earliest literature was carried out by Greco and Wright [11] and Sardisco, et al., [12] who found that a protective sulfide film formed at concentrations of H₂S < 1,700 ppm corresponding to gas pressure of < 0.1 psia. At higher concentrations, a nonprotective sulfide film was reported. Videm and Kvarekval also observed that small concentrations of H₂S (0.02 mmol or 0.0065 psi) decreased the corrosion rate of steel at 70°C and 80°C in a 1 M NaCl solution with 10 psi CO₂ [13]. However, pitting corrosion occurred in these solutions, possibly caused by selective dissolution of the ferrite phase. At higher H₂S concentrations (0.002 psi to 0.0082 psi), considerable scatter in corrosion rate was observed, with the corrosion rate generally increasing with H₂S concentration. At the natural pH of the H₂S and CO₂ solutions (~4), the film formed was not visible and no evidence of sulfides was found. At a pH of 6.9, a thick corrosion product was observed, which consisted of a mixture of FeS, FeCO₃, and pyrrhotite. Ho-Chung-Qui and Williamson reported that, in an environment containing H₂S/CO₂ at the ratio of ~4, chloride concentration > 10,000 ppm caused severe localized corrosion. The corrosion was associated with the presence of ferrous chloride (FeCl₂), which formed as a layer between iron sulfide and the metal.

Oxygen is also a critical incentive of corrosion inside gas pipeline. However, the only presence of it cannot claim the dominance. Thus, very few studies of the effect of O₂ have been reported in the literature. Durr and Beavers examined the effect of various O₂ concentrations in a 1200 psi gas mixture consisting of 1% CO₂ and 3.76 ppm H₂S above a stagnant solution (flowing gas mixture) of 1 wt% NaCl [14]. Results show that the corrosion rate was highest at the vapor/liquid interface. The corrosion rate was significant (0.086 mm/y overall corrosion rate and 0.356 mm/y at the vapor/liquid interface) even at the lowest O₂ concentration studied (10 ppm), and there was a gradual increase in penetration with O₂ concentration.

Lyle and Schutt showed that, while the formation of iron sulfide films decreased corrosion rates, the sulfide film was not completely protective, as evidenced by localized corrosion [15]. Buffering the

solutions to a pH of 6 resulted in a marked decrease in uniform and localized corrosion rate. Chloride increased the localized corrosion rate. Slowly flowing solution increased general corrosion rates and reduced the pitting susceptibility of carbon steel relative to stagnant conditions. Under slowly flowing conditions, the presence of O₂ increased the corrosion rate significantly and enhanced localized corrosion. Specimens were more susceptible to pitting corrosion on portions of partially immersed specimens exposed to the vapor phase. Pitting occurred on fully immersed specimens in only 1 of 11 test conditions, while on the vapor phase portions of partially immersed specimens pitting occurred in 7 of the 11 test conditions. Severe pitting occurred on steel surfaces exposed to the vapor phase when O₂ at a concentration of 100 ppm by volume (ppmv) or 1,000 ppmv was present as the only constituent in the gas being used in the tests. When 0.5 psi H₂S was combined with 100 ppmv or 1,000 ppmv of O₂, severe corrosion of steel surfaces exposed in the vapor phase resulted. In the absence of O₂, 0.5 psi H₂S had little effect on steel corrosion rates. Increasing CO₂ partial pressures tended to increase general corrosion rates of carbon steel and made it more susceptible to pitting, particularly on portions of specimens exposed to the vapor phase. The experimental data of fully immersed specimens yielded a statistical regression equation for general corrosion as followed:

$$CR = 8.7 + 9.86 \times 10^{-3}(O_2) - 1.48 \times 10^{-7}(O_2)^2 - 1.31(pH) + 4.93 \times 10^{-2}(CO_2)(H_2S) - 4.82 \times 10^{-5}(CO_2)(O_2) - 2.37 \times 10^{-3}(H_2S)(O_2) - 1.11 \times 10^{-3}(pH)(O_2) \quad (Eq.2)$$

The adjusted regression coefficient value (R²) for Equation 2 was 0.6235. It indicates that O₂ is the most important accelerator of corrosion, that there is a synergistic action between H₂S and CO₂ in increasing corrosion rate, and that increasing pH results in a decrease in corrosion rate. Unlike the DeWaard, et al., equation (Eq.1), no direct effect of CO₂ partial pressure was found under the conditions examined. Lyle and Schutt conducted one test for a longer period of time (1 month vs. the 14 days for all other tests) and found that the general corrosion rates increased with time whereas pitting rate (pit depth divided by total test time) decreased [15]. This would suggest that the corrosion occurred mostly under a nonprotective film and any “localized” corrosion was caused by the nonuniform nature of the corrosion product formed.

2.1.2 Literature review on Prototype Model on H₂S corrosion

To study the synergy of CO₂, H₂S and O₂ in pipeline corrosion rate, N. Sridhar and D.S.Dunn conducted experimental examinations using carbon steel samples [16]. Since the findings of this reference is very important for the understanding of H₂S corrosion, in this report, we detailed the experimental setup and the results in this reference so that it can guide us for our future tests. In Reference [16], 1080 Carbon Steel was used with chemical composition in Table 2 and the chemical solutions for lab experiments were shown in Table 3 [16]. In Reference [16], the cylindrical specimens of Type 1018 carbon steel (AISI 1018 Carbon Steel) (Table 2) were exposed to stagnant aqueous solutions saturated with gas mixtures containing 0.5 psia H₂S, 10 psia CO₂, and 100 ppmv O₂, in addition to high-purity nitrogen in an amount sufficient to maintain a total pressure of 500 psi. High-purity nitrogen was used instead of methane (CH₄) to reduce the risk of exceeding the flammability limit for O₂-CH₄ gas mixtures. Tests were conducted in stagnant solutions because in many gathering and transmission lines, stagnant or slow flow conditions cause high corrosion rates; stagnant conditions tend to maximize the scale-forming tendency, and operational difficulties with the plugging of transfer lines in the laboratory system by scale were encountered. Reference [16] reported the measured pH values after the tests, along with the detected reaction products using Raman Spectroscopy method. There was a reasonable agreement between the measured and calculated values in pH value, but an obviously more diverse reaction product.

Table 2 Chemical Composition of 1018 Carbon Steel [16]

Element	Composition (wt%)								
	C	Si	Mn	S	P	Cr	Cu	Ni	Al
	0.18	0.2	0.7	0.007	0.005	0.01	0.05	0.02	<0.004

Table 3 Compositions of the solutions in distinguished cases [16]

Case #	Composition	pH Value
1	166 g CaCl ₂ , 58.4 g NaOH, 10 psi CO ₂ , 0.5 psi H ₂ S, 100 ppm O ₂	11.5
2	166 g CaCl ₂ , 0.821 g NaOH, 10 psi CO ₂ , 0.5 psi H ₂ S, 100 ppm O ₂	5.4
3	235 g MgCl ₂ , 0.78 g NaOH, 10 psi CO ₂ , 0.5 psi H ₂ S 100 ppm O ₂	5.1
4	15 g CaSO ₄ , 0.372 g NaOH, 10 psi CO ₂ , 0.5 psi H ₂ S, 100 ppm O ₂	5.6
5	30 g NaCl, 1.289 g NaHCO ₃ , 10 psi CO ₂ , 0.5 psi H ₂ S, 100 ppm O ₂	5.6
6	285 g CaCl ₂ , 102 g MgCl ₂ , 7.7 g KCL, 351 g NaCl, 0.639 g NaOH, 10 psi CO ₂ , 0.5 psi HV, 100 ppm O ₂	5.5
7	285 g CaCl ₂ , 102 g MgCl ₂ , 7.7 g KCl, 351 g NaCl, 0.209 g NaOH, 10 psi CO ₂ , 0.5 psi HV, 100 ppm O ₂	4.8
8	30 g NaCl, 0.346 g NaOH, 10 psi CO ₂ , 0.5 psi HV, no O ₂	5.2
9	30 g NaCl, 0.346 g NaOH, 10 psi CO ₂ , no O ₂	5.1
10	0.283 g NaOH, 10 psi CO ₂ , 0.5 psi HV, no O ₂	5.0

Table 4 Results of Corrosion Tests [16]

Case #	Final pH	Gas pressure (psi)	Corrosion Rate (mm/y)		Detected Solids	Predicted Solids
			CR (Fully immersed)	CR (Partially immersed)		
1	11.5	CO ₂ : 10 H ₂ S: 0.5 O ₂ (ppmv): 100	0.064	0.11	CaCO ₃ FeCO ₃ β-FeOOH Fe _{1+x} S	Fe _{1+x} S CaCO ₃
2	5.4	CO ₂ : 10 H ₂ S: 0.5 O ₂ (ppmv): 100	0.139	0.067	FeCO ₃ β-FeOOH γ-FeOOH	Fe _{1+x} S
3	5.1	CO ₂ : 10 H ₂ S: 0.05 O ₂ (ppmv): 100	0.058	0.043	Unassigned Peaks	Fe _{1+x} S
4	5.6	CO ₂ : 10 H ₂ S: 0.5 O ₂ (ppmv): 100	0.147	0.47	CaSO ₄ CaCO ₂	Fe _{1+x} S CaSO ₄
5	5.6	CO ₂ : 10 H ₂ S: 0.5 O ₂ (ppmv): 100	0.17	0.54	MCO ₃ MHCO ₃ γ-FeOOH β-FeOOH	Fe _{1+x} S
6	4.9	CO ₂ : 10 H ₂ S: 0.5 O ₂ (ppmv): 100	0.107	0.067	γ-FeOOH γ-Fe ₂ O ₂ Fe _{1+x} S	Fe _{1+x} S
7	4.8	CO ₂ : 10 H ₂ S: 0.5 O ₂ (ppmv): 100	0.13	0.11	β-FeOOH γ-FeOOH	Fe _{1+x} S
8	5.2	CO ₂ : 10 H ₂ S: 0.5 O ₂ (ppmv): 0	0.21	0.079	Fe _{1+x} S γ-FeOOH	Fe _{1+x} S
9	5.1	CO ₂ : 10 H ₂ S: 0 O ₂ (ppmv): 0	0.35	0.043	FeCO ₃ γ-FeOOH	FeCO ₂
10	4.9	CO ₂ : 10 H ₂ S: 0.5 O ₂ (ppmv): 100	0.176	0.26	Fe _{1+x} S	Fe _{1+x} S

In addition, Reference [16] also performed exposure tests simultaneously in 3 L of solution in Type 316L (UNS S31603) stainless steel autoclaves. The temperature within the cell containing the autoclaves was maintained at $15.5 \pm 1^\circ\text{C}$ ($60 \pm 2^\circ\text{F}$). Premixed gases containing required concentrations of H_2S , CO_2 , and O_2 were continuously flowed through liquids in the autoclaves at 10 mL/min. At the completion of a test and prior to cleaning the specimen, Reference [16] performed Raman spectroscopy and x-ray diffraction (XRD) analyses on selected specimens to characterize the chemical compositions of deposits formed on specimen surfaces. Through all the applied test above, graphical results were adopted to evaluate the contribution of CO_2 and H_2S to the promotion of in-line corrosion rate under certain pH values. As shown in Figure 1, generally, increasing of the pH resulted in a decrease in corrosion. The result showed that the corrosion rate in chloride-free solutions under a variety of gas mixtures was generally lower when the pH was increased to 6. The test conducted at pH 11.5 had a solution with 3.53 wt% chloride. The large scatter in the data makes an unequivocal conclusion of the role of pH on corrosion difficult. However, it was clear from the figure that when the pH value is 6, either of the gas component is contributive to the inner corrosion of tested carbon steel.

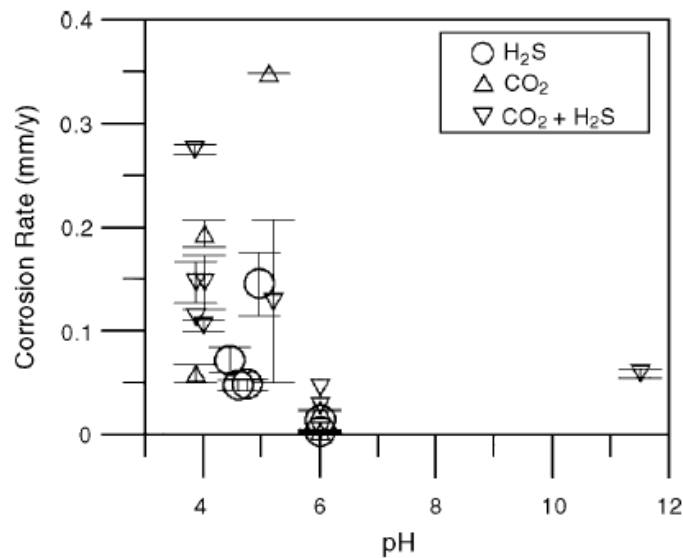


Figure 1 Effect of pH on general corrosion rate of fully immersed specimens [16]

In addition of the measurement of CR, Reference [16] also investigated the polarization behavior of steel using a typical cyclic potentiodynamic polarization curve shown in Figure 2, indicating a completely active behavior. In the H_2S environment, the increase in polarization at high current densities was essentially the result of transport-limited dissolution rather than protective film formation or a large ohmic component. The potential-current density relationship was not linear, and there was a slight hysteresis in the polarization behavior. The transport-limiting process was not determined in this study, but could be the diffusion of dissolved $\text{Fe}(\text{HS})^+$ complexes away from the electrode. The lack of passivity was evident not only in the shape of the polarization curves, but also in the lack of significant hysteresis between the forward and backward scans. Typically, if passive films exist and localized corrosion was observed, significant hysteresis in the polarization curves would occur. The lack of passive behavior indicated that the scale or corrosion products formed on the steel may have provided minimal protection. The presence of oxygen in the gas phase increased the corrosion potential significantly, as shown in Figure 3. This indicated that O_2 promotes corrosion through cathodic depolarization.

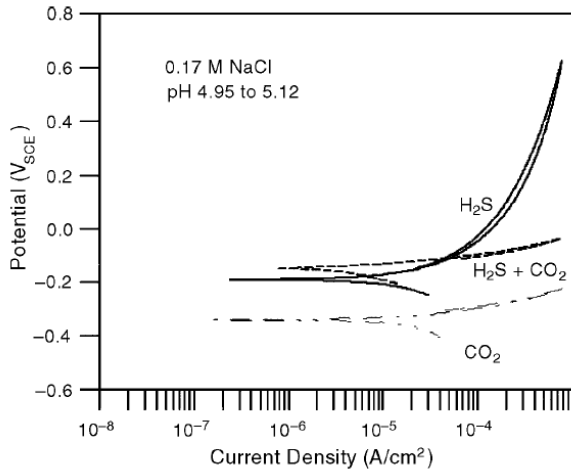


Figure 2 Cyclic potentiodynamic polarization curves of steel in various environments [16]

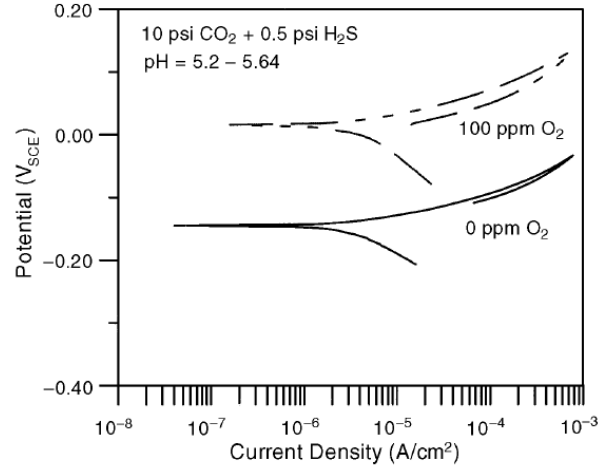


Figure 3 Cyclic potentiodynamic polarization curves of steel vs. O₂ concentration in the gas [16]

Reference [16] let us know that the empirical models developed through limited tests are not valid beyond the range of factors used to develop the models. Thus, the DeWaard, et al., model cannot be used in environments containing H₂S in addition to CO₂. By the same token, the empirical model developed by Lyle and Schutt cannot be used in an environment without H₂S and O₂ because the model does not indicate a dependence on CO₂ alone. Though there is still not a model indicating the CR by those gas components, these literatures have provided a reachable direction of what should be considered when doing research on the pipeline inner-surface corrosion. Thus, under this background, Obanijesu E. O. has developed a corrosion model considering the only contribution of H₂S [17]. In Reference [17], a basic expression (Eq. 3) for the corrosion rate was adopted by considering pH, gas fugacity and wall shear stress based on Norsork Standard (NS, 2005) [18]. Equation 3 illustrated the CR at 20°C ≤ T ≤ 150°C:

$$CR_T = K_T f_i \left(\frac{s}{19} \right)^{0.146 + 0.0324 \log f_i} f(pH) t \text{ (mm/year)}. \quad (\text{Eq.3})$$

In this equation, K_T is temperature constant varies from temperature, and the specific values are presented in Reference [18]. The parameters in Equation (3) were considered as follow:

- a) pH: H₂S is soluble in water to give a weak acid and pH plays a significant role in pipeline corrosion rate. The mathematical formulation for determining the pH effect, $f(pH)$ is a function of pH and temperature given by Dugstad et al [19]. For example, at temperature ranges 20°C ≤ T ≤ 150°C, and pH value is determined under room temperature (20°C), the real pH value ($f(pH)$) in the solution is:

When 20°C ≤ T ≤ 60°C,

$$f(pH) = 2.0676 - 0.2309pH \quad (pH \geq 3.5) \quad (\text{Eq.4})$$

$$f(pH) = 5.1885 - 1.2353pH \quad (pH \geq 4.6) \quad (\text{Eq.5})$$

When 60°C ≤ T ≤ 150°C,

$$f(pH) = 0.836 - 0.1818pH \quad (pH \geq 3.5) \quad (\text{Eq.6})$$

$$f(pH) = 15.444 - 6.1291pH + 0.0708pH^2 \quad (pH \geq 4.6) \quad (\text{Eq.7})$$

b) The shear stress in pipeline walls: The wall shear stress as one of the parameters needed to calculate corrosion rate [18] is a function of friction factor f , mixture density ρ_m , and superficial velocity U_m , and it is expressed by [18] as:

$$S = 0.5\rho_m f \cdot U_m \quad (\text{Eq.8})$$

In which, the mixture density is,

$$\rho_m = \rho_L\lambda + \rho_G(1 - \lambda) \quad (\text{Eq.9})$$

Velocity is,

$$U_m = U_L^s + U_G^s \quad (\text{Eq.10})$$

And viscosity is,

$$\mu_m = \mu_L\lambda + \mu_G(1 - \lambda) \quad (\text{Eq.11})$$

In these equations, λ is given as:

$$\lambda = \frac{Q_L}{Q_L + Q_G} \quad (\text{Eq.12})$$

where μ_G is the viscosity of gas (Ns/m²), μ_L is the viscosity of liquid (Ns/m²), μ_w is the viscosity of water (Ns/m²), Q_G is the volumetric flow rate of gas (m³/s), Q_L is the volumetric flow rate of liquid, ρ_G , ρ_L and ρ_m are density of gas, liquid, and their mixture, respectively. U_m is the mixed or equivalent velocity.

c) Fugacity: Gases (H₂S) are not ideal at high pressure, so to compensate for this, the partial pressure of a gas is multiplied by a fugacity constant. Prausnitz [20] expresses fugacity as:

$$f_i = aP_i \quad (\text{Eq.13})$$

where the partial pressure P_i is:

$$P_i = \frac{\text{Mass flow of } i \text{ in the gas (Kmole/h)} \times \text{Total pressure}}{\text{Total mass flow in the gas phase (Kmole/h)}} \quad (\text{Eq.14})$$

The fugacity coefficient (a) is given by deWaard et al. as a function of temperature and pressure as:

$$a = 10^{P(0.0031 - \frac{1.4}{T})}, \text{ when } P \leq 250 \text{ bar} \quad (\text{Eq.15})$$

$$a = 10^{2.5(0.0031 - \frac{1.4}{T})}, \text{ when } P \geq 250 \text{ bar} \quad (\text{Eq.16})$$

Based on all the Equations above, Reference [17] provided a computer program to solve the solution. The influencing trend of each parameter in the empirical equation are shown in Figure 4 to 8. Figure 4 showed that corrosion rate increases with temperature, which perfectly agrees with the study carried out by Nuclear Power Fundamental (NPF, 2006a) [21]. This could be attributed to its (temp) secondary effects through its influence on the solubility of the corroding agent, which was the most common factor

influencing corrosion. This showed that when the operating temperature changes, so many other factors, which affect the rate of corrosion will change, some in the same direction while some in the opposite direction. This confirmed that with temperature corrosion rate increases.

From Figure 5, increase in wall shear stress increased corrosion rate. Corrosion could be accelerated by stress either by residual internal stress in the pipe or external applied stress (Ginzel and Kanfers) [22]. Residual stresses were produced by deformation during fabrication, unequal cooling from high temperature and/or by internal structure arrangements involving volume change. Obstacles and other geometrical changes in the flow would give rise to higher shear stress. Furthermore, different flow regime and geometrical obstacles might generate shear stress fluctuations where the shear stress peaks might be considerably higher than the average shear stress.

Corrosion rate also increased with superficial velocity as shown by Figure 6, which agreed with Hsu and Adamson [23]. Though change in velocity was a method employed in preventing pipeline erosion attack (which is the destruction of a metal by abrasion or attrition caused by the fluid flow with or without suspended solids), it, however, had an adverse impact on the internal property of the pipe by increasing the corrosion rate since an increase in the relative movement between a corrosive solution and metallic surface tended to accelerate corrosion.

Figure 7 showed that pH had a serious impact on the eventual rate at which corrosion increased longitudinally; this also agreed with the acidic part of NPF [21]. The relationship depended on the soluble corroding agent and the type of metal used for the pipe's construction. If the metal was acid soluble (such as iron), the corrosion rate was controlled by the rate of transport of available oxidizer to the metal surface; amphoteric metals (such as aluminum and zinc) dissolved rapidly in the acidic or basic solution aiding the corrosion while noble metals (such as gold and platinum) were not appreciably affected by pH.

Fugacity had a profound effect on the corrosion rate as confirmed by Figure 8 where corrosion rate increased with fluid fugacity. This could strongly be attributed to the relationship between the temperature and fugacity as shown by various equations in the developed simulation technique. This also confirmed the existence of temperature difference between the internal system and the surrounding. The fugacity did not have a constant internal interval even when the pressure was set to be constant. Corrosion rates increased with increase in fugacity at least for the range examined.

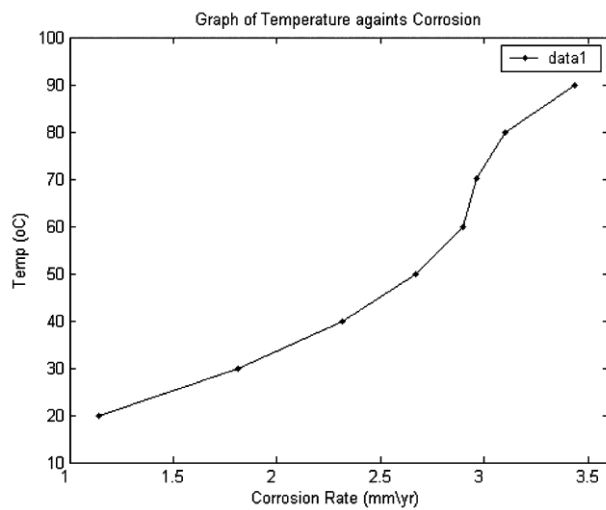


Figure 4 Temperature vs. CR [17, 21]

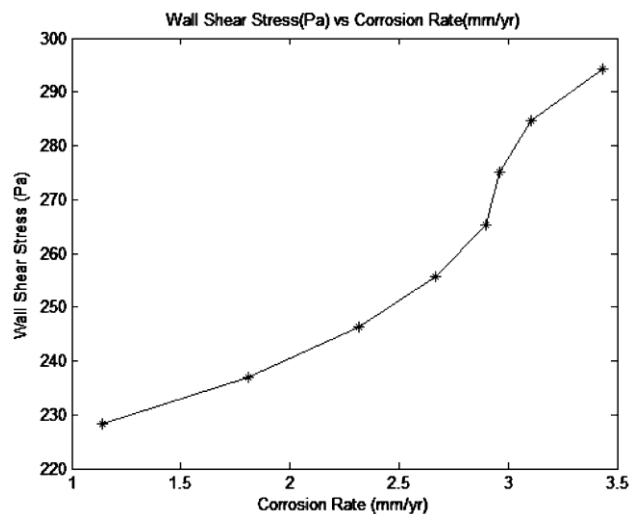


Figure 5 Wall shear stress vs. CR [17, 22]

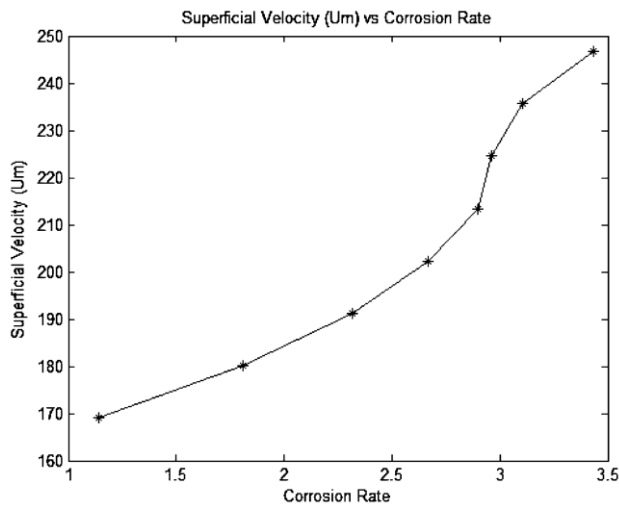


Figure 6 Superficial velocity vs. CR [17, 23]

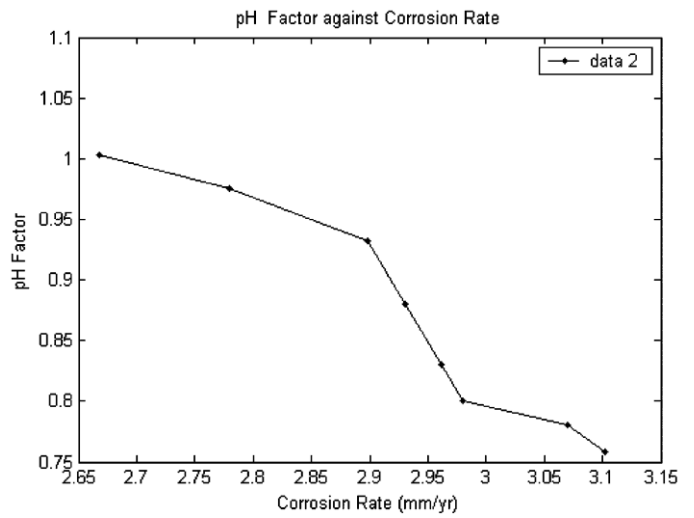


Figure 7 pH vs. CR [17, 21]

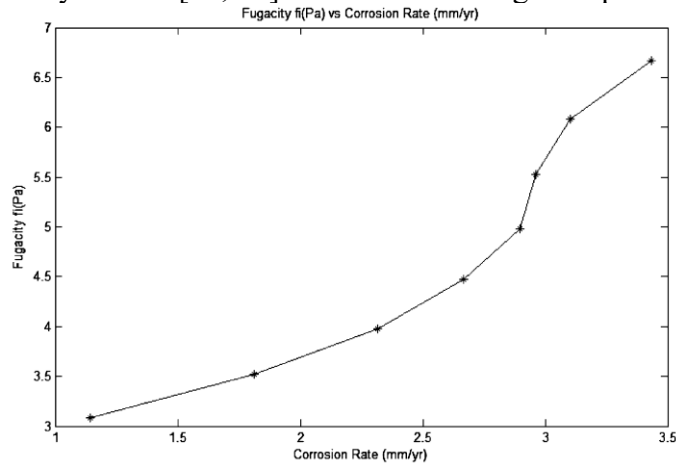


Figure 8 Fugacity vs. CR [17]

All the above literature reviews give us guidance on the selection of parameters and their ranges to be considered in the corrosion prediction model with consideration of corrosive water. In next quarter, based on these literature review, the selected corrosion models in this section will be used to predict corrosion rates with the detected corrosive parameters from the developed sensor arrays. Laboratory experiments will be conducted to evaluate the effectiveness of the use of such a model to predict the corrosion in such a detected corrosive environment.

2.3 Student Mentoring

students (Shuomang Shi, Ph. D. in Civil and Environmental Engineering at NDSU, Hafiz Usman Ahmed, Masters in Civil and Environmental Engineering at NDSU, and Jiapeng Lu, Ph.D. Student in chemistry at NDSU) continue working on this project. The three graduate students will work on this project from Quarter 7 to Quarter 8 of this project. New undergraduate research assistants will be hired in Sep 2020 for future quarters of this project.

2.4 Outreach Activities

In this quarter, we planned an outreach event to Native American community, with collaboration to “NATURE Sunday Academy” Program at NDSU. The outreach was planned in detail in this quarter and will be performed in next quarter.

2.5 Future work

In the 8th quarter, we will resume the four objectives planned in Quarter 6th:

- 1) Task 2.1: Develop sensor film for the H⁺/pH;
- 2) Task 2.2: Continue the simulation and experimental research on the survivability under oil/gas or water environment;
- 3) Task 2.2: Test and analyze more sensor film characteristics and continue quantify the color changes;
- 4) Task 3: Test parameters for corrosion model prediction.

References:

- [1] F.F. Lyle, H.C. Burghard, Jr., E.P. George, Project No. 730-FFES-FUC-85 Albany, NY: New York State Energy Development Authority, 1990.
- [2] C. de Waard, D.E. Milliams. 1975. Prediction of Carbonic Acid Corrosion in Natural Gas Pipelines in CO₂ Corrosion in Oil and Gas Production (Houston, TX: NACE, 1984), p. 506-510.
- [3] C. de Waard, U. Lotz, A. Dugstad, "Influence of Liquid Flow Velocity on CO₂ Corrosion: A Semi-Empirical Model," CORROSION/ 95, paper no. 128 (Houston, TX: NACE, 1995).
- [4] C.A. Palacios, Y. Hernandez, "Application of Simulation Techniques for Internal Corrosion Prediction," CORROSION/97, paper no. 2 (Houston, TX: NACE, 1997).
- [5] D.W. Shoesmith, P. Taylor, M.G. Bailey, B. Ikeda, *Electrochem. Acta* 23 (1978a): p. 903-916.
- [6] D.W. Shoesmith, M.G. Bailey, B. Ikeda, *Electrochem. Acta* 23 (1978b): p. 1,329-1,339.
- [7] J.S. Smith, J.D.A. Miller, *Brit. Corros. J.* 10, 3 (1975): p. 136-143.
- [8] D.W. Shoesmith, P. Taylor, M.G. Bailey, D. Owen, *J. Electrochem. Soc.* 127 (1980): p. 1,007-1,015.
- [9] H.H. Huang, W.T. Tsai, J.T. Lee, *Corrosion* 52, 9 (1996): p. 708-713.
- [10] X.L. Cheng, H.Y. Ma, J.P. Zhang, X. Chen, S.H. Chen, H. Q. Yang, *Corrosion* 54, 5 (1998): p. 369-376.
- [11] E.C. Greco, W.B. Wright, *Corrosion* 18 (1962): p. 119t-124t.
- [12] J.B. Sardisco, W.B. Wright, E.C. Greco, *Corrosion* 19 (1963): p. 354t.
- [13] K. Videm, I. Kvarekval, *Corrosion* 51, 4 (1995): p. 260-269.
- [14] C.L. Durr, J.A. Beavers, "Effect of Oxygen on the Internal Corrosion of Natural Gas Pipelines," CORROSION/96, paper no. 612 (Houston, TX: NACE, 1996).
- [15] F.F. Lyle, H.U. Schutt, "CO₂/H₂S Corrosion Under Wet Gas Pipeline Conditions in the Presence of Bicarbonate, Chloride, and Oxygen," CORROSION/98, paper no. 11 (Houston, TX: NACE, 1998).
- [16] N. Sridhar, D. S. Dunn, A. M. Anderko, M. M. Lencka, H. U. Schutt, Effects of Water and Gas Compositions on the Internal Corrosion of Gas Pipelines—Modeling and Experimental Studies, CORROSION. 2001;57(3):221-235.
- [17] ObaniJesu, E. O., and Sonibare, J. A. 2005. Natural gas flaring and environmental protection in Nigeria. *NAFTA J.* 56:287–294.
- [18] Norsork Standard (NS). 2005. CO₂ Corrosion Rate Calculation Model, 20Majorstural, Norway: Norwegian Technological Standards Institute Oscarsgt.

- [19]Dugstad, A., Lunde, L. and Videm, K. 1994. Parametric study of CO₂ corrosion of carbon steel, Houston, Texas: National Association of Corrosion Engineers (NACE). Paper No. 14
- [20]Prausnitz, J. M. 1999. Molecular Thermodynamics of Fluid-Phase Equilibria. Quebec, Canada: Prentice-Hall International Inc.
- [21]Nuclear Power Fundamentals (NPF). 2006b. Effect of pH on the corrosion rate of iron in water, accessed on September 22, 2006
- [22]Ginzel, R. K. and Kanters, W. A. 2002. Pipeline corrosion and cracking and the associated calibration considerations for same side sizing applications.
- [23]Hsu, P. C. and Adamson, M. G. 1999. FY99 Final report for the expedited technology demonstration project: Demonstration test results for the MSO/off-gas and salt recycled system U.S. Department of Energy Contract W-7405-ENG-48